JOURNAL OF GEOPHYSICAL RESEARCH, VOL. 95, NO. B6, PAGES 8607–8615, JUNE 10, 1990

A Possible Explanation for Foreland Thrust Propagation

JOHN PANIAN AND WALTER PILANT

Department of Geology and Planetary Sciences, University of Pittsburgh, Pennsylvania

A common feature of thin-skinned fold and thrust belts is the sequential nature of foreland directed thrust systems. As a rule, younger thrusts develop in the footwalls of older thrusts, the whole sequence propagating towards the foreland in the transport direction. As each new younger thrust develops, the entire sequence is thickened; particularly in the frontal region. The compressive toe region can be likened to an advancing wave; as the mountainous thrust belt advanced the down- surface slope stresses drive thrusts ahead of it much like a surfboard rider. In an attempt to investigate the stresses in the frontal regions of thrustsheets, a numerical method has been devised from the algorithm given by *McTigue and Mei* [1981]. The algorithm yields a quickly computed approximate solution of the gravity- and tectonic-induced stresses of a two-dimensional homogeneous elastic half-space with an arbitrarily shaped free surface of small slope. A comparison of the numerical method with analytical examples shows excellent agreement. The numerical method was devised because it greatly facilitates the stress calculations and frees one from using the restrictive, simple topographic profiles necessary to obtain an analytical solution. The numerical version of the McTigue and Mei algorithm shows that there is a region of increased maximum resolved shear stress, τ, directly beneath the toe of the overthrust sheet. Utilizing the Mohr-Coulomb failure criterion, predicted fault lines are computed. It is shown that they flatten and become horizontal in some portions of this zone of increased τ. Thrust sheets are known to advance upon weak decollement zones. If there is a coincidence of increased τ, a weak rock layer, and a potential fault line parallel to this weak layer, we have in place all the elements necessary to initiate a new thrusting event. That is, this combination acts as a nucleating center to initiate a new thrusting event. Therefore, thrusts develop in sequence towards the foreland as a consequence of the stress concentrating abilities of the toe of the thrust sheet. The gravity- and tectonic-induced stresses due to the surface topography (usually ignored in previous analyses) of an advancing thrust sheet play a key role in the nature of shallow foreland thrust propagation.

INTRODUCTION

Chapple [1978] has listed 4 characteristics that are fundamental to any thin-skinned fold-and-thrust belt; (1) they are thin-skinned; i.e., folding and faulting occur in the stratigraphic section at some level above the basement rocks, (2) the thin-skinned belt is bounded by a basal layer composed of particularly weak rock or a zone of high pore fluid pressure, (3) the belt before and after deformation is wedged shaped, (4) the whole wedge has been systematically shortened and thickened. In his classic study of the eastern margin of the Canadian Rocky Mountains, *Dahlstrom* [1970] gives two geometric rules concerning thrust systems that can be generally applied to any foreland fold-and-thrust belt; (1) thrusts cut up-section in the direction of tectonic transport, (2) thrusts tend to be parallel to bedding in weak, incompetent layers and oblique to stronger, more competent ones.

Individual thrusts can join into a thrust system forming either an imbricate fan or a duplex [*Boyer and Elliott,* 1982]. In an imbricate fan, each thrust has an asymptotic shape that curves downward to a common basal sole thrust (see Figure 1a). Should a series of imbricate slices be bounded on the top by the original thrust surface, the structure is termed a duplex (see Figure 1b). On the basis of stratigraphic and geometric evidence, *Elliott* [1980, p.187] is led to state that

> Thrusts develop in sequence toward the foreland...Each individual thrust moves into place and thickens the section, particularly in its imbricate frontal region; then this entire mass moves on a newer and lower fracture surface, with the imbrications now incorporated into a larger thrust sheet.

This sequential nature of foreland thrusting, i.e., thrusts generally propagating outward from the hinterland towards the foreland, has been documented by many authors; *Bally et.al.* [1966] and *Dahlstrom* [1970] for the Canadian Rockies, and *Armstrong and Oriel* [1965] for the Idaho-Wyoming thrust belt are some of the more common studies cited in the literature. (There are exceptions, of course, such as overstep thrust sequences [*Boyer and Elliott,* 1982], but it is our understanding that these are the exceptions and not the rule [see *Butler,* 1982, p.241].) A satisfactory explanation for this sequential, systematic development of foreland thrust systems has not been presented.

Davis et.al. [1983] present a model in which the overall mechanics of fold-and-thrust belts are analagous to a wedge of soil or snow in front of a moving bulldozer. However, they do not provide an explanation as to how individual thrusts are systematically developed at the toe. *Mandl and Shippam* [1981] provide a scenario in which they predict imbrication in a thrust sheet in terms of areas of high critical strength values in the sheet. But, as mentioned before, they neglect any topography that may be produced by the successive imbrication of the sheet. Thus, their original stress field distributions cannot be applied to subsequent imbrications as they attempt to do in their model.

There are several recent studies dealing with the forces necessary for thrust sheet emplacement; whether gravitational or longitudinal compressive forces are the dominant cause. For the frontal portions of thrust sheets,

Paper number 90JB00356.
0148-0227/90/90JB-00356$05.00

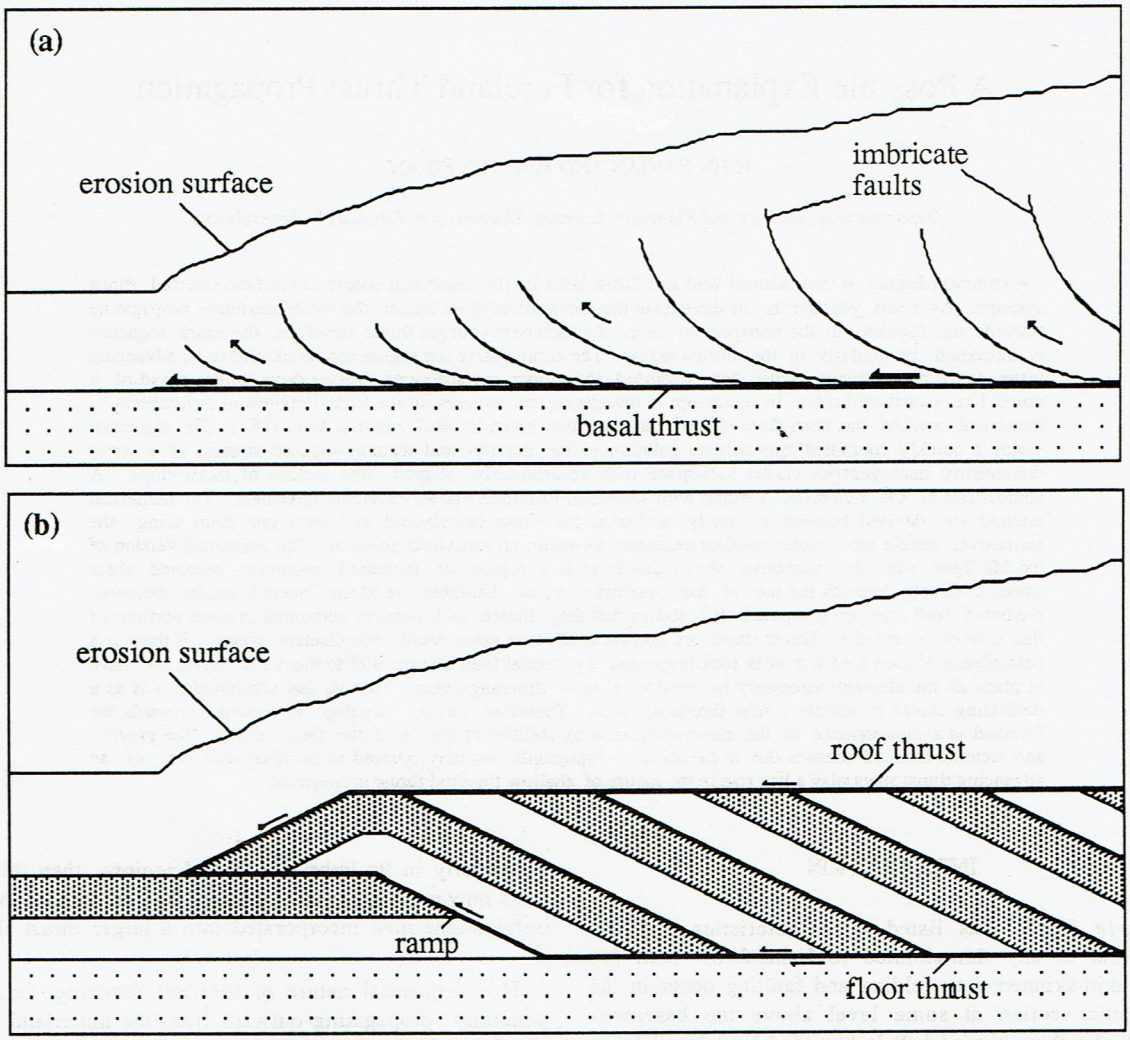

Fig. 1. (a) Illustration of an imbricate fan. Faulting proceeded from right to left. (b) Illustration of a duplex. Faulting proceeded from right to left.

longitudinal compressive forces are clearly important [*Elliott* 1976b, 1980]. These forces may be the result of a 'push' applied in the hinterland [*Chapple*, 1981; *Davis et.al.*, 1983] or from the gravitational 'spreading' of the mountainous mass [*Elliott*, 1976a].

THE EFFECTS OF TOPOGRAPHIC RELIEF

Topography is an important element in any analysis of stress distribution in the upper crust [*Elliott*, 1976a]. The usual calculations for the effect of topographic relief rely on a zeroth order approximation which says that the normal stress component at the surface ($y = 0$) of a half space is related to the topographic loading and that the tangential stress component is zero. Clearly, these are not the relevant equations. One must find a solution which allows the vanishing of the stresses upon the topographic surface, $h(x)$, itself . Previous analyses dealing with stress distributions and subsequent prediction of thrust faulting have been unsatisfactory since the gravitational spreading of a topographic load produces significant shear tractions and cannot be ignored. For example, *Hafner's* [1951] analysis, which is often cited in the literature, and *Mandl and Shippam's* [1981], both ignore the presence of any surface slope. It is unrealistic to do so.

An analytical solution to gravitationally induced stresses in the presence of topographic irregularities has been given by *Savage, Swolfs, and Powers* [1985] and a similar solution for the stress concentration due to the stress concentrating abilities of topographic discontinuities was given shortly thereafter by *Savage and Swolfs* [1986]. These particular forms of solution (obtained by conformal mapping) have as a significant advantage, exactness. They have as a disadvantage that there are only a small number of analytical types of topography subject to easy conformal transformation. Somewhat earlier, *McTigue and Mei* [1981] had provided a (first order) approximation to the exact solution which is useful when topographic slopes are small. This algorithm also suffers from the need to have topographic representations which are sufficiently simple to be amenable to the evaluation of Hilbert transforms related to functions of this topography. However, their algorithm has a major advantage in that it can be evaluated numerically (with insignificant loss of accuracy). This means that one can calculate stress values in the case of arbitrary (subject to the small slope limitation) topographic surface representations. This is the

major reason for the use of this approximate algorithm. As with most first order approximations, there is difficulty in obtaining a measure of its accuracy. We shall say more about this later.

Not only did these three papers show that shear tractions could not be ignored in the case of topographically induced stresses and stress concentrations, but the *McTigue and Mei* [1981] paper also showed that accurate results may not agree with commonly accepted knowledge. For example, they found that in the case of a ridge, there was horizontal compression near the crest and that in the case of a valley, there would be tension at the bottom. These first order results were confirmed by *Savage, Swolfs, and Powers* [1985] using an exact solution.

One can make a model (in light of their results) to suggest why this might be so. In Figure 2a, it is clear that the force of gravity acting on the slope materials would induce tensile stresses at the top of a ridge. On further consideration, we see that the bending moment induced by flattening will induce the opposite, i.e., compressive forces. At this point intuition fails us. Which will win out? The paper cited tells us that the bending moment is more important. Similarly, with the bending moment created in the valley case, the bottom will thus be in a state of tension (Figure 2b).

An analytical approximation

Utilizing the observation that a wide variety of topographic features are characterized by small slopes, *McTigue and Mei* [1981] have employed a perturbation scheme to obtain integral representations (accurate to first order) for the stresses in the near surface vicinity in a region with topographic relief. Their analysis assumes a two-dimensional homogeneous elastic half-space with an arbitrarily shaped free surface. A Cartesian coordinate system is defined with y, the vertical axis, taken as positive upwards and x, the horizontal axis, increasing positively to the right. Stress, σ_{ij}, is normalized by $\rho g H$, where ρ = density, g = the acceleration of gravity, and H = the characteristic height of the topography. The coordinates are made dimensionless by normalizing x and y by L, the characteristic length of the topography. The characteristic slope of the topography is thus defined as $\varepsilon = H/L$ with the requirement that $H/L \ll 1$. Figure 3 illustrates the coordinate system utilized. Their results can be written as (M&M followed by a number refer to equations found in *McTigue and Mei* [1981]:

$$\text{M\&M(18)} \quad \sigma_{yy} = \frac{y}{\varepsilon} - h + O(\varepsilon^2)$$

$$\text{M\&M(22)} \quad \sigma_{xx} = \frac{\nu}{1-\nu}\frac{y}{\varepsilon} - h + \varepsilon\frac{2-3\nu}{2-2\nu}\frac{1}{\pi}\int_{-\infty}^{\infty}\overline{h^2}|\xi|e^{-i\xi x}d\xi$$

$$-\int_{-\infty}^{\infty}\bar{h}\,|\xi|e^{-i\xi x}d\xi + O(\varepsilon^2)$$

$$\text{M\&M(23)} \quad \sigma_{xy} = -\varepsilon\frac{2-3\nu}{2-2\nu}\frac{\partial(h^2)}{\partial x} + y\frac{\partial h}{\partial x} + O(\varepsilon^2)$$

$\bar{h}$ and $\overline{h^2}$ are the Fourier transforms of $h(x)$ and $[h(x)]2$, respectively. The effect of the distributed shear is represented by terms quadratic in h and the distributed normal load is represented by terms multiplied by y.

As noted in the introduction, longitudinal compressive forces must also be considered. *McTigue and Mei* [1981] continued their analysis to allow for the superposition of a uniform far-field tectonic compression (or tension) on the gravitationally induced stress field. Their results giving the stresses related to a far-field tectonic stress are:

$$\text{M\&M(52)} \quad \sigma^t_{yy} = 0 + O(\varepsilon^2)$$

$$\text{M\&M(53)} \quad \sigma^t_{xx} = R\left[1 - \varepsilon\frac{1}{\pi}\int_{-\infty}^{\infty}\bar{h}\,|\xi|e^{-i\xi x}d\xi\right]$$

$$\text{M\&M(54)} \quad \sigma^t_{xy} = \varepsilon R\frac{\partial h}{\partial x} + O(\varepsilon^2)$$

where R is the ratio of the tectonic stress to the gravitational stress ($R = \sigma_\infty/\rho g H$); $R > 0$ for regional

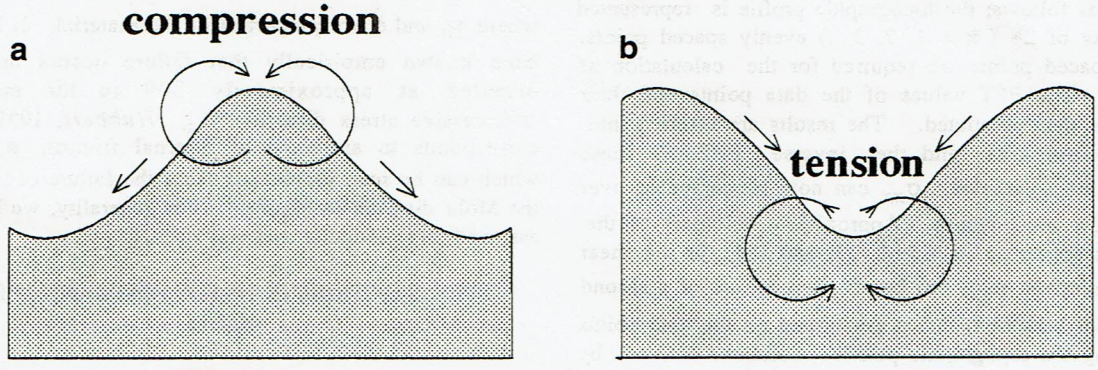

Fig. 2. Competing factors, gravitational sliding and bending moments, in ridge and valley. In both cases, the bending moment is more influential and leads to compression at the top of the ridge and tension in the valley bottom.

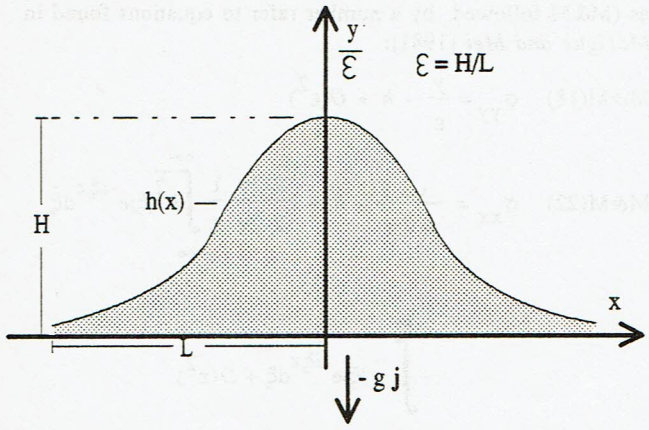

Fig. 3. Coordinate system and parameters used in stress calculations.

tension and $R < 0$ for regional compressional. To obtain both the stresses due to the gravitational body force and the tectonic force, one simply adds M&M (18, 22, 23) to M&M (52, 54). This set of equations allows the representation of the complete distribution for the leading edge of a thrust sheet.

A numerical implementation

To evaluate these expressions for a given function $h(x)$, one must obtain the necessary transforms and inverse transforms appearing in these equations. This can be done for a few simple topographies [several examples appear in *McTigue and Mei*, 1981] but the analytical expressions they obtained are not amenable to the insertion of arbitrarily prescribed topographic relief. This limitation can be removed by making a numerical implementation of the analytical results. The rapid evaluations of transforms and related quantities can be affected by the use of the Fast Fourier Transform (FFT) using a discretization fine enough to remove discernable differences between analytical and numerical results.

The computation of M&M (18) for the vertical stress component, σ_{yy}, is straightforward; simply subtract the topographic height from the vertical height at the corresponding horizontal distance. Taken over a grid of points in the x and y directions, a two dimensional representation of σ_{yy} is obtained. The FFT is utilized in the numerical evaluation of the integrals and transforms appearing in M&M (22) and (52). The procedure is briefly described as follows; the topographic profile is represented by an array of 2^k (k = 1, 2, 3,...) evenly spaced points. (Evenly spaced points are required for the calculation of the FFT.) The FFT values of the data points and their squares are then computed. The results are inserted into M&M(22) and (52) and the inverse FFT of these quantities are calculated. σ_{xx} can now be computed over the grid of x and y values. Approximate solutions of the derivatives appearing in M&M (23) and (54) for the shear stress component, σ_{xy}, can be obtained by use of a second order Taylor series expansion performed on the data points representing the topographic profile. Solutions derived by the above methods have been compared with the analytical solutions for an example given in *McTigue and Mei* [1981, Figure 4] and show excellent agreement. A computer program that computes these stress components as well as other stress related quantities will be the subject of a forthcoming paper.

STRESS DISTRIBUTION AND FAULTING

The analysis of stress in an elastic, homogeneous body is well known [e.g., *Jaeger and Cook*, 1976]. Now that the stress components can be computed at any point utilizing the numerical methods described above, it is a simple procedure to calculate the remaining relevant stress quantities to obtain a complete representation of the stress field. The principal stress axes are the two mutually perpendicular directions across which the shear stresses vanish. The principal stress magnitudes are given by

$$\sigma_1 = \frac{1}{2}(\sigma_{xx}+\sigma_{yy}) + \left[\sigma_{xy}^2 + \frac{1}{4}(\sigma_{xx}-\sigma_{yy})^2\right]^{1/2}$$
$$\sigma_3 = \frac{1}{2}(\sigma_{xx}+\sigma_{yy}) - \left[\sigma_{xy}^2 + \frac{1}{4}(\sigma_{xx}-\sigma_{yy})^2\right]^{1/2} \quad (1)$$

Here we use the convention that compressive stresses are negative and tensile stresses positive. (This is opposite that commonly used in geologic analyses, but the same as used by *McTigue and Mei* [1981].) Thus, σ_3 is the maximum compressive stress and σ_1 the least compressive stress. The principal stress directions are given by

$$\tan 2\theta = \frac{2\sigma_{xy}}{\sigma_{xx}-\sigma_{yy}} \quad (2)$$

where θ is the counter-clockwise angle that they make with the positive x-axis. The maximum shear stress, or stress difference, at any point is

$$\tau = \left[\sigma_{xy}^2 + \frac{1}{4}(\sigma_{xx}+\sigma_{yy})^2\right]^{1/2} = \frac{\sigma_1 - \sigma_3}{2} \quad (3)$$

Faulting is more likely to occur first in regions where τ attains its highest values since material bodies fail in shear rather than in compressive collapse. With the introduction of internal friction, this highest value is somewhat greater than τ_{crit} given by the Mohr-Coulomb fracture criterion:

$$\tau_{crit} = \tau_0 + \sigma_n \tan\phi \quad (4)$$

where τ_0 and ϕ are properties of the material. It has long been known empirically that failure occurs on planes oriented at approximately 30° to the maximum compressive stress direction [e.g., *Hubbert*, 1951]. This corresponds to an angle of internal friction, ϕ, of 30° which can be seen graphically from the failure condition of the Mohr diagram in Figure 4. For generality, we have not assumed and particular material strength.

STRESS DISTRIBUTIONS FOR FORELAND THRUST SHEETS

Several hypothetical profiles representing the topography of an advancing thrust sheet are presented in Figures 5a-c. They are based on previously published

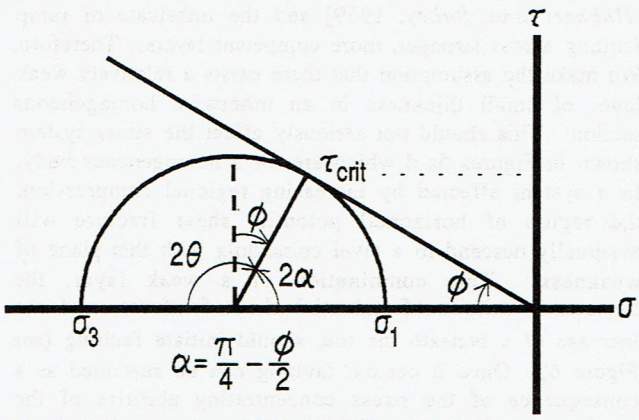

Fig. 4. Mohr-Coulomb conditions for failure. With increasing stress levels, the circle expands until fracture occurs just as it becomes tangent to the critical line given by equation (4) of the text.

examples [see *Elliott*, 1976b; *Johnson*, 1981; *Willemin*, 1984]. The three profiles vary in their degree of slope, especially in the steepness at the toe. The stress components were calculated over a grid of evenly spaced points within the profiles. From these values, contours of τ, the maximum shear stress, were plotted. In Figures 5a through 5c, regional compression was applied while in Figure 5d there was no horizontal compression. (The topographic profile in Figure 5d was the same as in Figure 5c. The effects were similar for the other two profiles and so are not presented.) The amount of horizontal compression is measured by the ratio of regional compression to the maximum vertical compression due to material between the reference level ($y = 0$) and the maximum topographic height, H, and is expressed by $R = \sigma/\rho g H$. This ratio, R, is -0.5 in Figures 5a-c, and zero in

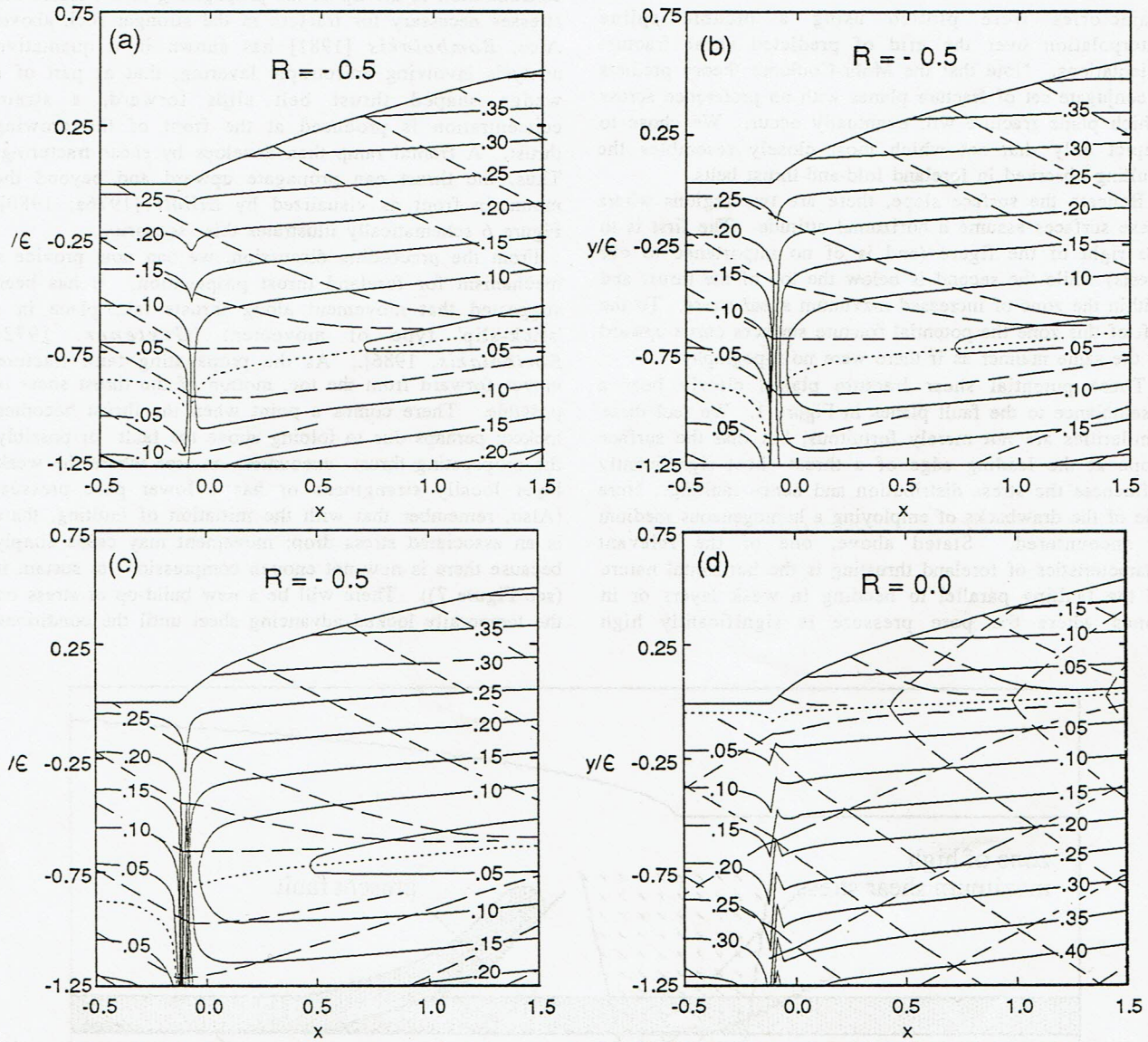

Fig. 5 (a)-(d). Stress profile beneath a foreland thrust sheet. Solid lines represent contours of maximum shear stress τ, broken lines represent potential fracture trajectories, and the dashed line is where the horizontal and vertical stresses are equal. Dipping contours of shear stress represent a ridge of increased shear stress (above the dashed line) while rising contours below the line also represent increased shear stress. Basal slope of the thrust sheet toe increases from Figure 5a to Figure 5c. The factor $R = (\sigma_\infty/\rho g H) = -0.5$ represents a level of regional stress in which the horizontal compression is 1/2 the gravitational compression due to ridge topography. (d) Same as Figure 5c except $R = 0$, i.e., there is no regional compression.

Figure 5d. (The choice of -0.5 is suggested by *Elliot* [1976a, p.956)]. The effect of adding horizontal compression is to increase the shear stress values near the surface and to decrease them at depth.

In all examples, a minimum of τ is located in the region where σ_{yy} becomes equal to σ_{xx} (see (3)) and shown as the dashed line in Figures 5a-d. Where there is an applied regional stress, there is a very marked increase in τ beneath the toe. When there is no regional stress, Figure 5d, this increase still occurs but is greatly reduced. This region of increased stress is very important and will be discussed further on.

Broken lines represent the predicted surfaces of shear fracture. These are oriented at an angle, α, to the σ_3 direction where $a = \pm[\pi/2 - \phi/2]$. For $\phi = 30^o$, $\alpha = 30^o$. The σ_3 direction is given by (2). These potential fracture trajectories were plotted using a bicubic spline interpolation over the grid of predicted shear fracture orientations. Note that the Mohr-Coulomb theory predicts a conjugate set of fracture planes with no preference across which plane fracture will eventually occur. We chose to depict only that set which most closely resembles the faulting observed in foreland fold-and-thrust belts.

Beneath the surface slope, there are two regions where these surfaces assume a horizontal attitude. The first is to the right of the figure (and is of no importance to our thesis) while the second is below the toe of the thrust and within the zone of increased maximum shear stress. To the left of this zone the potential fracture surfaces curve upward in the same manner as if there were no topography.

These potential shear fracture planes clearly bear a resemblance to the fault planes in Figure 1. We feel these similarities are not merely fortuitous, but that the surface slope at the leading edge of a thrust sheet significantly influences the stress distribution and hence faulting. Here one of the drawbacks of employing a homogeneous medium is encountered. Stated above, one of the relevant characteristics of foreland thrusting is the horizontal nature of the faulting parallel to bedding in weak layers or in zones where the pore pressure is significantly high [*Hubbert and Rubey*, 1959] and the imbricate or ramp faulting across stronger, more competent layers. Therefore, We make the assumption that there exists a relatively weak layer of small thickness in an otherwise homogeneous section. This should not seriously affect the stress system shown in Figures 5a-d which are for a homogeneous body. In a system affected by increasing regional compression, the region of horizontal potential shear fracture will eventually descend to a level coinciding with this plane of weakness. This combination of a weak layer, the horizontal attitude of potential shear fractures, and the increase of τ beneath the toe, should initiate faulting (see Figure 6). Once it occurs, faulting can be sustained as a consequence of the stress concentrating abilities of the crack edge representing the laterally propagating thrust fracture [*Elliott*, 1976b; *Gallagher and Rizer*, 1977].

The zone of high τ beneath the toe plus the stress concentration at the tip of the propagating thrust create the stresses necessary for fracture in the stronger rock above. Also, *Bombolakis* [1981] has shown in a quantative analysis involving anisotropic layering, that as part of a wedge shaped thrust belt slips forward, a strain concentration is produced at the front of the growing thrust. A frontal ramp then develops by shear fracturing. Thus, the thrust can propagate upward and beyond the mountain front as visualized by *Elliott* [1976a; 1980]. Figure 6 schematically illustrates this scenario.

From the preceeding discussion, we can now provide a mechanism for foreland thrust propagation. It has been suggested that movement along thrusts take place in a 'stick-slip' type of movement [*Gretener*, 1972; *Bombolakis*, 1986]. As the propagating fault fracture moves forward from the toe, motion of the thrust sheet is possible. There comes a point when the thrust becomes locked; perhaps due to folding above the fault or possibly the propagating thrust encounters an area where the weak layer locally strengthens or has a lower pore pressue. (Also, remember that with the initiation of faulting, there is an associated stress drop; movement may cease simply because there is now not enough compression to sustain it (see Figure 7)). There will be a new build-up of stress on the temporaily locked advancing sheet until the conditions

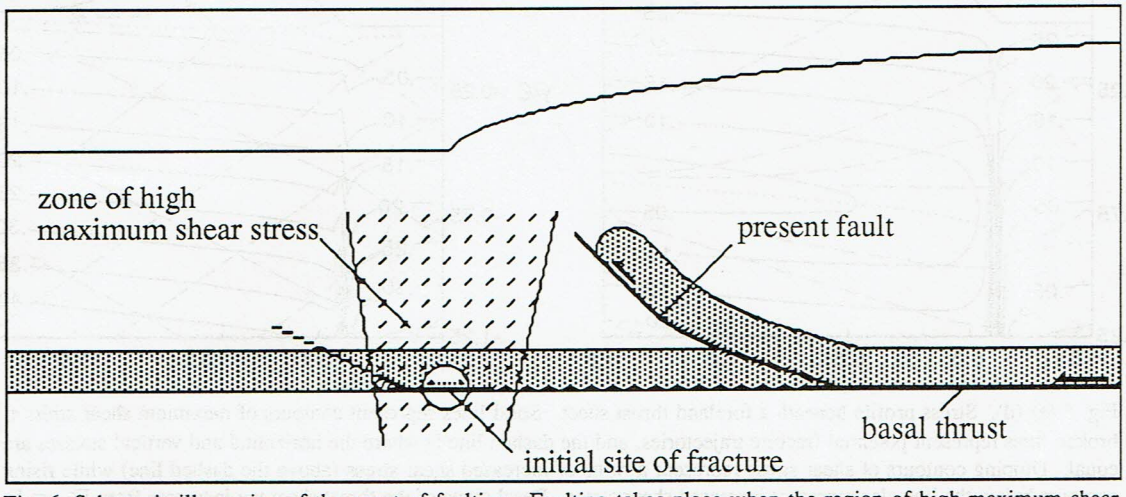

Fig. 6. Schematic illustration of the onset of faulting. Faulting takes place when the region of high maximum shear stress, weakened rock zone (decollement), and horizontal potential fracture trajectory coincide. Heavy lines represent existing faults and broken lines future faults. The dotted arrow shows sense of fracture propagation of the new fault.

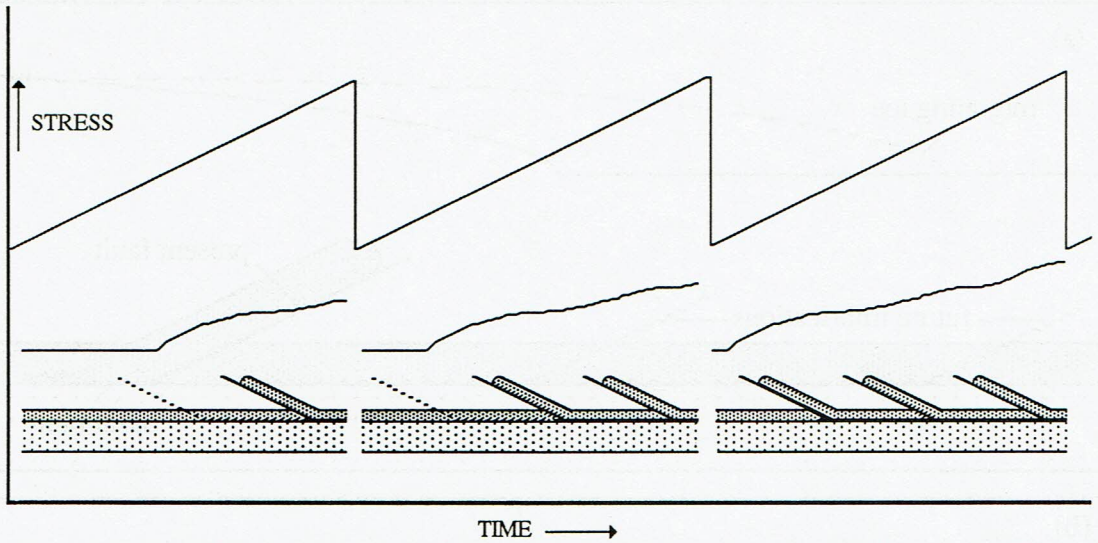

Fig. 7. Time sequence of stick-slip movement of thrusting as a consequence of stress variation through time. The upper curve represents a steadily increasing level of regional stress which is suddenly reduced as a new thrust occurs. While the regional stress is still at low levels (steadily increasing, however) healing is taking place along the upward ramp, strengthening it so that the weakest rocks remain in the decollement zone. As a critical regional stress level is reached, fracture occurs at a new point beneath the toe of the thrust sheet. Dashed lines represent future faults.

described above are encountered anew. The process is repeated as long as there exists a strong enough 'push' from the hinterland. The sequential nature of foreland thrust propagation can be visualized as a consequence of a migrating toe (see Figures 8a-b). The 'surfrider' analogy of Haarman as interpreted by *Elliott* [1976a] is therefore appropriate. The advancing surface slope of a thrust sheet ('the wave') drives thrusts ('surfboards') ahead of it as a consequence of the stress concentrating abilities of the advancing toe region of the thrust sheet.

Limitations of the model

Both the approximate algorithm and its numerical implementation can be used only when the slopes are small. (Active thrusting in the Transverse Ranges of Southern California has maximum slopes on the order of 20^{o}. These would make severe demands on the first order approximation. However, the time sequence we propose would have new thrusting taking place after a period of time (healing) in which such steep scarps would be reduced by erosion. One can only guess what they would be, but reductions to 1/3 or 1/4 of that value do not seem unreasonable. These reduced slopes of 5 to 7 degrees are more in line with the requirements of the approximate algorithm.) On the other hand, this implementation has a beneficial result for the numerical work in that the discrete samples will never have to represent a steep slope.

Another difficulty is clearly evident using the *McTigue and Mei* [1981] algorithm; their analysis assumes a homogeneous, elastic solid and neglects the finite thickness of the elastic lithosphere. This will result in an error in the stress field at depth. However, for topographies with a typical length scale comparable to or less than this thickness, the needed correction should be insignificant [*McTigue and Mei*, 1981, p. 9269]. Thus in this study, with horizontal length scales on the order of tens of kilometers, this omission is inconsequent.

In assuming a homogeneous elastic solid, the presence of anisotropic strata and the existence of any previous faulting or deformation is obviously ignored. Incorporating such inhomogeneities would present formidable obstacles toward a final solution. Neverless, the previous simplified analysis yields some important insights concerning foreland thrusting.

CONCLUSIONS

Two important results have been obtained in the preceding discussion. The first is that a numerical implementation has been devised for the *McTigue and Mei* [1981] algorithm allowing its use in more general applications. That is, one can now include arbitrarily specified topography in the determination of gravity- and tectonic-induced stresses. Secondly, we have found a plausible explanation for the sequential nature of foreland thrusting.

The numerical algorithm given here eliminates the necessity of employing only those topographic models from which analytical results may be derived. Such models are generally described by simple polynomials and trigonometric functions and thus are limited in the topographic structures they may represent. The numerical algorithm is subject to no such difficulties, being limited only by the fundamental requirement that the topographic slope is small.

Secondly, it has previously been recognized that the topography developed during thrusting significantly modifies the stress field [*Elliott*, 1976b; *Willemin*, 1984]. With the aid of this numerical algorithm, we have computed the stress fields for hypothetical topographic profiles produced by an advancing thrust sheet. These allow significant insights can be made as to the sequential nature of foreland thrusting. Summarizing:

1. Thrust faulting is initiated beneath the toe of an advancing thrust sheet as a result of high τ concentrations and the horizontal sense of potential shear fracturing located at depth.

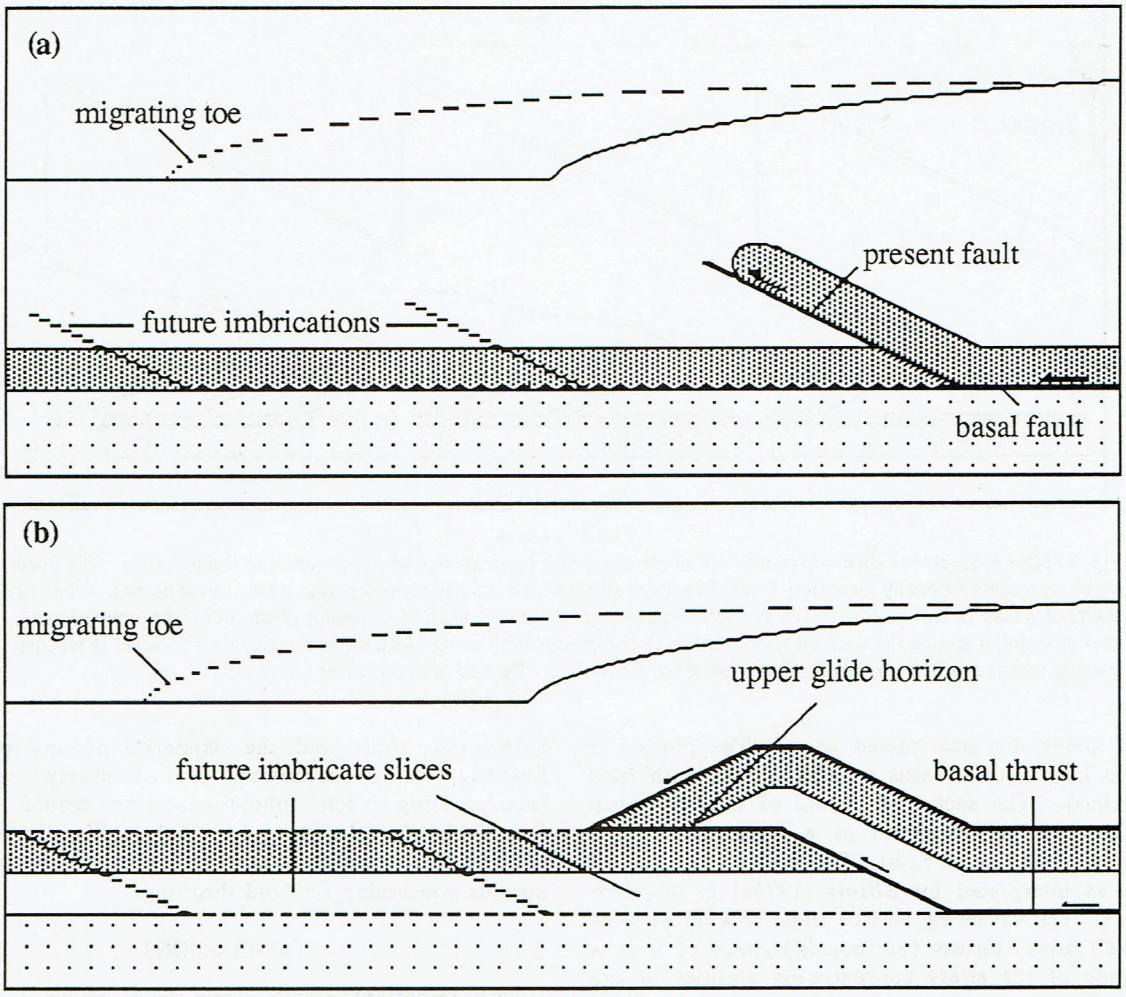

Fig. 8. (a) Schematic representation of foreland thrust propagation in the development of an imbricate fan. (b) Schematic representation of foreland thrust propagation in the development of a duplex.

2. Individual thrusts propagate towards the foreland, ahead of the advancing thrust sheet, due to the migrating toe of the thrust sheet.

3. The formation of entire thrust systems can be visualized in terms of the 'surfrider' analogy; thrusts develop progressively ahead of preceeding ones, toward the foreland, as the toe of the thrust sheet advances.

4. The shear stresses built up by gravitation are much smaller than those developed by a concentration of regional compression. Consequently, it would appear that regional compression must be the primary factor in the formation of a thrust system.

Acknowledgments. The authors are grateful to D.F. McTigue and an anonymous reviewer for their helpful comments and suggestions in reviewing this paper.

REFERENCES

Armstrong, F.C., and S.S. Oriel, Tectonic development of Idaho-Wyoming thrust belt, *Bull. Am. Assoc. Pet. Geol., 49,* 1847-1866, 1965.

Bally, A.W., P.L. Gordy, and G.A.Steward, Structure, seismic data and orogenic evolution of southern Canadian Rockies, *Bull. Can. Pet. Geol., 14,* 337-381, 1966.

Bombolakis, E.G., Thrust-fault mechanics and origin of a frontal ramp, *J. Struct. Geol., 8,* 281-290, 1986.

Boyer, S.E., and D. Elliott, Thrust systems, *Bull. Am. Assoc. Pet. Geol., 18,* 1196-1230, 1982.

Butler, R.W., The terminology of structures in thrust belts, *J. Struct. Geol., 4,* 239-245, 1982.

Chapple, W.M., Mechanics of thin-skinned fold-and-thrust belts, *Geol. Soc. Am. Bull., 89,* 1189-1198, 1978.

Dahlstrom, C.D.A., Structural geology in the eastern margin of the Canadian Rocky Mountains, *Bull. Can. Pet. Geol., 18,* 332-406, 1970.

Davis, D.J., J. Suppe and F.A. Dahlen, Mechanics of fold-and-thrust belts and accretionary wedges, *J. Geophys. Res., 88,* 1153-1172, 1983.

Elliott, D.E., The motion of thrust sheets, *J. Geophys. Res., 81,* 949-963, 1976a.

Elliott, D.E., The energy balance and deformation mechanisms of thrust sheets, *Proc. R. Soc. London, Ser. A, 283,* 289-312, 1976b.

Elliott, D.E., Mechanics of thin-skinned fold-and-thrust belts: Discussion, *Geol. Soc. Am. Bull., 91,* 185-187, 1980.

Gallagher, J.J., and W.D. Rizer, Photoelastic model studies of thrust fault initiation, *Wyoming Geol. Ass. Guidebook. 29th Annual Conference,* 441-118, 1977.

Gretener, P.E., Thoughts on overthrusting in a layered sequence, *Bull. Can. Pet. Geol., 20,* 583-607, 1972.

Hafner, W., Stress distributions and faulting, *Geol. Soc. Am. Bull., 62,* 373-398, 1951.

Hubbert, M.K., Mechanical basis for certain familiar geologic structures, *Geol. Soc. Am. Bull., 62,* 355-372, 1951.

Jaeger, J.C., and N.G.W. Cook, *Fundamentals of Rock Mechanics,* Halstead, New York, 1976.

Johnson, M.R.W., The erosion factor in the emplacement of the

Keystone thrust sheet (South East Nevada) across a land surface, *Geol. Mag., 118*, 501-507, 1981.

Mandl, G., and G.K. Shippam, Mechanical model of thrust sheet gliding and imbrication, *Thrust and Nappe Tectonics*, edited by K.R. McClay and N.J. Price, *Spec. Publ. Geol. Soc. London, 9*, 427-448, 1981.

McTigue, D.F., and C.C. Mei, Gravity-induced stresses near topography of small slope, *J. Geophys. Res., 86*, 9268-9278, 1981.

Savage, W.J., and H.S. Swolfs, Tectonic and gravitational stress in long symmetric ridges and valleys, *J. Geophys. Res., 91*, 3677-3685, 1986.

Savage, W.J., H.S. Swolfs, and P.S. Powers, Gravitational Stress in Long Symmetric Ridges and Valleys, *Int. J. Rock Mech. Min. Sci. Geomech. Abstr., 22*, 291-302, 1985.

Willemin, J.H., Erosion and the mechanics of shallow foreland thrusting, *J. Struct. Geol., 6*, 425-432, 1984.

J. Panian, UEC Environmental Systems, 600 Grant Street, Pittsburgh, PA 15222.

W. Pilant, Department of Geology and Planetary Sciences, University of Pittsburgh, Pittsburgh, PA 15260

(Received December 15, 1988;
revised January 29, 1990;
accepted November 18, 1989.)